Bright and Fast Emission from Robust Supramolecular J-aggregate Nanostructures through Silica-Encapsulation

Dimuthu H. Thanippuli Arachchi, Ulugbek Barotov, Collin F. Perkinson, Tara Šverko, Alexander E. K. Kaplan, Moungi G. Bawendi*

Department of Chemistry, Massachusetts Institute of Technology, 77 Massachusetts Avenue, Cambridge, Massachusetts, 02139, United States

*Corresponding Author: <u>mgb@mit.edu</u>

ABSTRACT

We introduce a two-step silica-encapsulation procedure to optimize both the optical efficiency and structural robustness of 5,5',6,6'-tetrachloro-1,1'-diethyl-3,3'-di(4-sulfobutyl)benzimidazolocarbocyanine (TDBC), a two-dimensional sheet-like J-aggregate. We report a fluorescence quantum yield of ~98%, the highest quantum yield recorded for any J-aggregate structure at room temperature, and a fast, emissive lifetime of 234 ps. Silica, as an encapsulating matrix, provides optical transparency, chemical inertness, and robustness to dilution, while rigidifying the J-aggregate structure. Our in situ encapsulation process preserves the excitonic structure in TDBC J-aggregates, maintaining their light absorption and emission properties. The homogeneous silica coating has an average thickness of 0.5-1 nm around J-aggregate sheets. Silica encapsulation permits extensive dilutions of J-aggregates without significant disintegration into monomers. The narrow absorbance and emission line widths exhibit further narrowing upon cooling to 79 K, which is consistent with J-type coupling in the encapsulated aggregates. This silica TDBC J-aggregate construct signifies (1) a bright, fast, and robust fluorophore system, (2) a platform for further manipulation of J-aggregates as building blocks for integration with other optical materials and structures, and (3) a system for fundamental studies of exciton delocalization, transport, and emission dynamics within a rigid matrix.

KEYWORDS: J-aggregates, silica-encapsulation, quantum yield, cyanine dyes, self-assembly

J-aggregates, supramolecular assemblies of organic molecules exhibiting distinctive optical properties, have emerged as interesting fluorophores because of their exceptional color purity and fast emissive lifetimes.¹⁻⁵ These aggregates typically form through the self-assembly of π conjugated chromophores, resulting in structures with distinct spectral shifts and enhanced lightharvesting capabilities. Initially, J-aggregates were observed independently by Jelley⁶ and Scheibe⁷ in the late 1930s. Ever since, supramolecular assemblies of cyanine dyes have sparked persistent curiosity due to their distinct exciton properties, diverging from the behavior of their constituent dye monomers. J-aggregates exhibit a high degree of organization with an array of morphologies including fibers, sheets, tapes, ribbons and nanotubes.^{3,8–11} The close alignment of chromophores within J-aggregates results in strong electronic state interactions, leading to supramolecular excitons spanning across multiple monomers. Superradiance occurs when the ensemble of aggregated chromophores collectively emits light coherently. 12 This cooperative emission causes redshifted and narrowed spectra¹³, extended exciton delocalization¹⁴, long-range exciton transport¹⁴⁻¹⁶, and notably sub-nanosecond emissive lifetimes^{12,17-19}. Leveraging these exceptionally distinct properties, J-aggregates have potential applications in sensing and imaging²⁰⁻²³ and are proposed as bright, fast, and ideal light sources for high-speed free-space optical^{24,25} and quantum communication.²⁶ However, despite their merits, J-aggregates still suffer from limitations that have hindered their use in devices and other applications. These limitations include low structural stability and low photoluminescence quantum yields (OYs).^{27,28} To address these limitations, we report a method that generates a bright and fast, sheet-like J-aggregate fluorophore, characterized by substantially improved structural robustness and close to unity QY.

The encapsulation of nanoparticles with a silica matrix marked a significant step in the advancement of nanomaterial engineering for optical applications. ^{29–32} Silica-encapsulation, with its well-established versatility and stability, also provides a protective and tunable environment for J-aggregates. Silica acts as an ideal encapsulating matrix for J-aggregates due to its optical transparency, chemical inertness, and ease of functionalization. 32-35 The integration of Jaggregates into silica matrices introduces a synergy, combining the distinctive characteristics of Jaggregates with the structural benefits of a silica host. This encapsulation strategy not only shields J-aggregates from external influences but also offers a platform for tailoring their optical properties, mechanical stability, and surface modifications while preserving their J-aggregate morphology and inherent optical properties. Silica-encapsulation of tubular C8S3 J-aggregates results in increased chemical and mechanical stability due to successful homogeneous and uniform silica-encapsulation.³⁵ These silica-stiffened C8S3 J-aggregates exhibit chemical stability against changes in pH in the medium and mechanical stability against drying. Yan Qiao et al. reported a QY enhancement in silica-encapsulated C8S3 J-aggregates with a photoluminescence QY of 8%, which is 1.3 times that of bare J-aggregates.³³ Silica-encapsulation of meso-tetrakis(4sulfonatophenyl) porphyrin (also known as TPPS) rod-like J-aggregate structures shows the ability of a silica shell with a controlled thickness to reinforce J-aggregate growth and to act as a perfect optical coupling spacer.³⁴

In this study, our focus centers on the enhancement of the structural robustness and optical efficiency of two-dimensional sheet-like 5,5',6,6'-tetrachloro-1,1'-diethyl-3,3'-di(4-sulfobutyl)benzimidazolocarbocyanine, commonly known as TDBC J-aggregates. TDBC dye molecules are known to self-assemble into 2D sheets spanning several hundred nanometers in water-methanol blends. These J-aggregates exhibit distinctive optical features from their constituent dye molecules, including extremely narrow absorption and emission spectra, rapid radiative rates, extensive exciton delocalization and excitation migration.^{36,37} In the past, the reported QYs for TDBC J-aggregates in solution were unsatisfactory, ranging from 5 to 49%, thus limiting their use in optical applications.³⁸⁻⁴⁰ However, we recently demonstrated a QY of 82% with a 174 ps emissive lifetime through the purification of monomers prior to their self-assembly. ²⁵ Purification of monomers enables successful removal of impurities embedded in the densely packed Jaggregate supramolecular lattice, which can trap excitons and function as non-radiative recombination centers. 25 While the optical performance of TDBC J-aggregates has improved, their persistent structural and chemical instability restricts their practical applications. This limitation also leaves room for further enhancement of their optical properties, including their fluorescence QY. To address this constraint, we devised a scheme to immobilize TDBC J-aggregates within a silica matrix using a two-step method that further increases the fluorescence QY.

Our study introduces a protocol for the silica-encapsulation of TDBC J-aggregate sheets using two silica precursors, namely, (3-aminopropyl)triethoxysilane and tetraethyl orthosilicate, in the presence of aqueous ammonia. The absorption and emission spectra exhibit no significant changes, indicating that silica-encapsulation has no effect on the existing excitonic structure or morphology of the TDBC J-aggregates. Microscopic analysis, including cryo-TEM images and scanning transmission electron microscopy with energy dispersive X-Ray analysis, confirm a successful and homogeneous silica coating on the J-aggregate sheets. Dynamic light scattering reveals a smaller lateral size for silica-coated J-aggregates than for bare J-aggregates, which is consistent with the short rod lengths reported for silica-encapsulated TPPS J-aggregates.³⁴ Stability studies involving dilution demonstrate that the enhanced structural integrity provided by silica coating helps to maintain the integrity of the J-aggregates, enabling extensive dilutions. In this study, we achieved a QY of 98% for TDBC J-aggregates, the highest recorded for any J-aggregate, through silicaencapsulation. The measured emissive lifetime is 234 ps. Our study marks a significant milestone for the development of J-aggregate systems as building block emissive materials, exhibiting a photoluminescence QY that is essentially unity at room temperature, reaching the limits of a bright, fast, and robust ideal fluorophore with enhanced processability.

RESULTS AND DISCUSSION

In situ two-step silica-encapsulation procedure and characterization of TDBC J-aggregates

The chemical structure of TDBC comprises a benzimidazole core with tetrachloro substituents, connected through a delocalized trimethine chain. Owing to the presence of the two sulfobutyl groups, the molecule shows a distinctive amphiphilic nature. The amphiphilic character arises from the coexistence of the hydrophilic sulfobutyl and hydrophobic tetrachloro-benzimidazole components within the same dye molecule. It imparts the ability for the molecule to interact with both polar and non-polar environments, facilitating its solubility in aqueous solutions while maintaining its compatibility with the organic phase. Previous studies have reported polymer coatings on J-aggregates utilizing such electrostatic interactions.⁴¹ The two-step silica-encapsulation procedure shown in Fig. 1A, uses the amphiphilicity of TDBC dye monomers to encapsulate TDBC sheet-like J-aggregates in amorphous silica. Our process was inspired by previous studies, including the controlled growth of silica in alcohol, the Stöber procedure,⁴² and silica-encapsulation of tubular and rod-shaped J-aggregates in water.^{32–35,42}

Our procedure is based on the sequential addition of amine-functionalized silane, (3aminopropyl)triethoxysilane (APTES) and tetraethyl orthosilicate (TEOS). In contrast to previous methods, during step-1 (Fig. 1A), in the presence of APTES, monomers undergo self-assembly. At first, due to the high affinity of the monomers to amines, TDBC will readily dissolve in APTES, creating monomer-rich regions, and eventually form two-dimensional sheet-like TDBC Jaggregates in the ultrapure water, resulting in a pink-colored homogeneous solution. Upon hydrolysis, APTES becomes adsorbed onto the negatively charged sulfonate groups projecting from both the top and bottom sides of the J-aggregate sheets through electrostatic interactions. Ideally APTES forms a monolayer, strategically covering the surface of TDBC sheets and acting as an anchoring group for the second silica precursor, TEOS, introduced in step-2 (Fig. 1A). TEOS contributes to the growth of the silica shell and by varying the TEOS concentration, the shell thickness can be controlled.³⁴ The addition of aqueous ammonia in step-2 serves a dual purpose: (i) It catalyzes the hydrolysis of silica precursors (APTES and TEOS) and triggers the cross-linking of silanes, resulting in the loss of ethane groups such as ethanol and the subsequent formation of silica, and (ii) the role of ammonium extends beyond base catalysis as it also serves to shield the silica coated J-aggregates from further aggregation and thus limits the physical size of the Jaggregates.43

The absorption (Figs. 1B, S1) and emission (Figs. 1C, S1) spectra of the silica-encapsulated TDBC J-aggregates are nearly identical in shape and position to those of the bare J-aggregate solutions. The consistent peak positions indicate that the excitonic structure of the bare J-aggregates remains unaffected by silica-encapsulation. However, the silica-encapsulated J-aggregates exhibit higher absorbance and emission intensities. This increase could be attributed to the higher abundance of J-aggregates formed in the presence of silica precursors as well as the enhanced radiative emission due to encapsulation. Cryo-TEM images (Figs. 1E, 1F) show two-dimensional sheet-like

morphologies for silica-encapsulated J-aggregates that are similar to those for bare J-aggregates but with greater abundance and smaller sizes. In the presence of silica precursors and aqueous ammonia, encapsulated J-aggregates are only several hundreds of nanometers in size, in contrast to the bare J-aggregates, which span more than a micron. The greater contrast observed for silica-encapsulated J-aggregates, due to the higher electron density caused by the silica sheath, provides a clear indication of a homogeneous silica coating on the surfaces of the J-aggregate sheets. Dynamic light scattering (DLS) autocorrelation curves (Fig. 1D) and normalized intensity distribution plots (Fig. S2) show a comparatively smaller size for silica-encapsulated J-aggregates, supporting Cryo-TEM observations.

Monomeric TDBC purified via our previously discussed procedure and dissolved in methanol²⁵ shows an orange color in the solution (Fig. 1G-I). An aliquot of dissolved monomers was added to a water/methanol mixture (12:1 v/v) to spontaneously form the J-aggregates (Fig. 1G-II), resulting in a pink solution. Once the two-step silica-encapsulation procedure is complete, bright pink silica-encapsulated J-aggregates (Fig. 1G-III) are formed. The increase in the intensity of the absorption and emission spectra of the silica-encapsulated TDBC J-aggregate sample in comparison to the bare J-aggregate sample, both of which were prepared from the same monomer dye concentration of 0.15 mM, indicates a boost in the formation of J-aggregates in the presence of silica precursors.³⁴ The absorption spectrum for bare J-aggregates shows a small peak around 517 nm, corresponding to the presence of non-aggregated TDBC monomers. This monomer peak is essentially nonexistent for silica coated J-aggregates, further confirming the increased growth of J-aggregates in the presence of silica precursors. As shown in Fig. 1A, self-assembly of TDBC monomers into J-aggregate sheets occurs in the presence of APTES. The electrostatically adsorbed cationic APTES promotes seeding and self-assembly by attracting free monomers through their sulfonate groups. The addition of ammonium during the second step prevents the agglomeration of silica-encapsulated J-aggregate sheets.

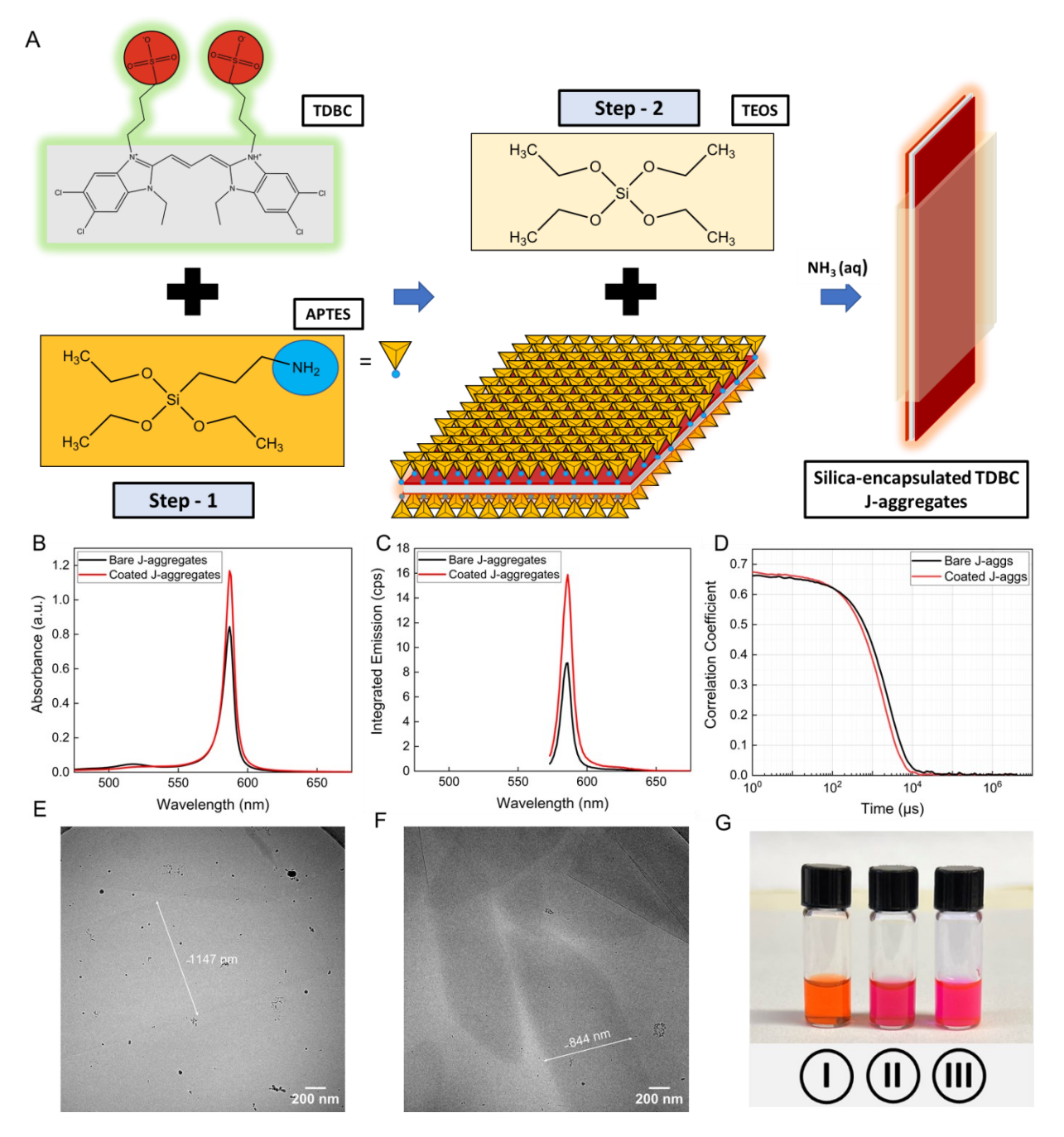


Figure 1. *In situ* two-step silica-encapsulation procedure and characterization of silica-encapsulated vs bare TDBC Jaggregates. (A) Schematic diagram of the two-step silica-encapsulation procedure in the presence of aqueous ammonia. (B) Steady-state absorption and (C) emission spectra for bare (black) and silica-encapsulated (red) J-aggregates. Normalized spectra are provided in Fig. S1. (D) DLS autocorrelation function: correlation coefficient as a function of time which describes the measured time-dependent fluctuations in light scattering intensity for bare (black) and silica-encapsulated (red) J-aggregates exhibiting smaller size for encapsulated J-aggregates. Normalized intensity distribution as a function of size is given under Fig. S2. (E), (F) Cryo-TEM images of bare and silica-encapsulated J-aggregates, respectively, further confirming the smaller size distribution for silica-encapsulated J-aggregate sheets. Scale bar: 200 nm. (G) Sample solutions of TDBC: I (left) - monomeric form in methanol: orange, II (middle) - J-aggregate form in water/methanol mixture (12:1 v/v): pink, III (right) - silica-encapsulated J-aggregates in aqueous solution: bright pink. Higher brightness in the J-aggregate sample to the right qualitatively indicates a higher fluorescence light output brought by silica-encapsulation.

Surface analysis of silica-encapsulated TDBC J-aggregate sheets

Silica-encapsulation preserves the excitonic structure and existing optical properties of bare J-aggregates while providing them with a protective and chemically tunable surface. Successful encapsulation should be homogeneous and should substantially cover both the top and bottom surfaces of the J-aggregate sheets. Figure 2 shows chemical, surface, and thickness analyses of silica-encapsulated and bare TDBC J-aggregates. We characterized the chemical composition of the silica-encapsulated TDBC J-aggregates using scanning transmission electron microscopy (STEM). STEM images are consistent with the elliptical shape of the silica-encapsulated TDBC J-aggregates observed *via* cryo-TEM (Fig. 1F). Figure 2A shows a high-angle annular dark-field (HAADF)-STEM image, and Figs. 2B, 2C show energy dispersive X-ray (EDX) elemental maps of silicon in the same field of view and an overlap of the silicon distribution map with the HAADF-STEM image, respectively. Fig. 2D presents an integral EDX spectrum showing silicon (Si) and oxygen (O) from silica-encapsulation and sulfur (S) and chlorine (Cl) from TDBC.

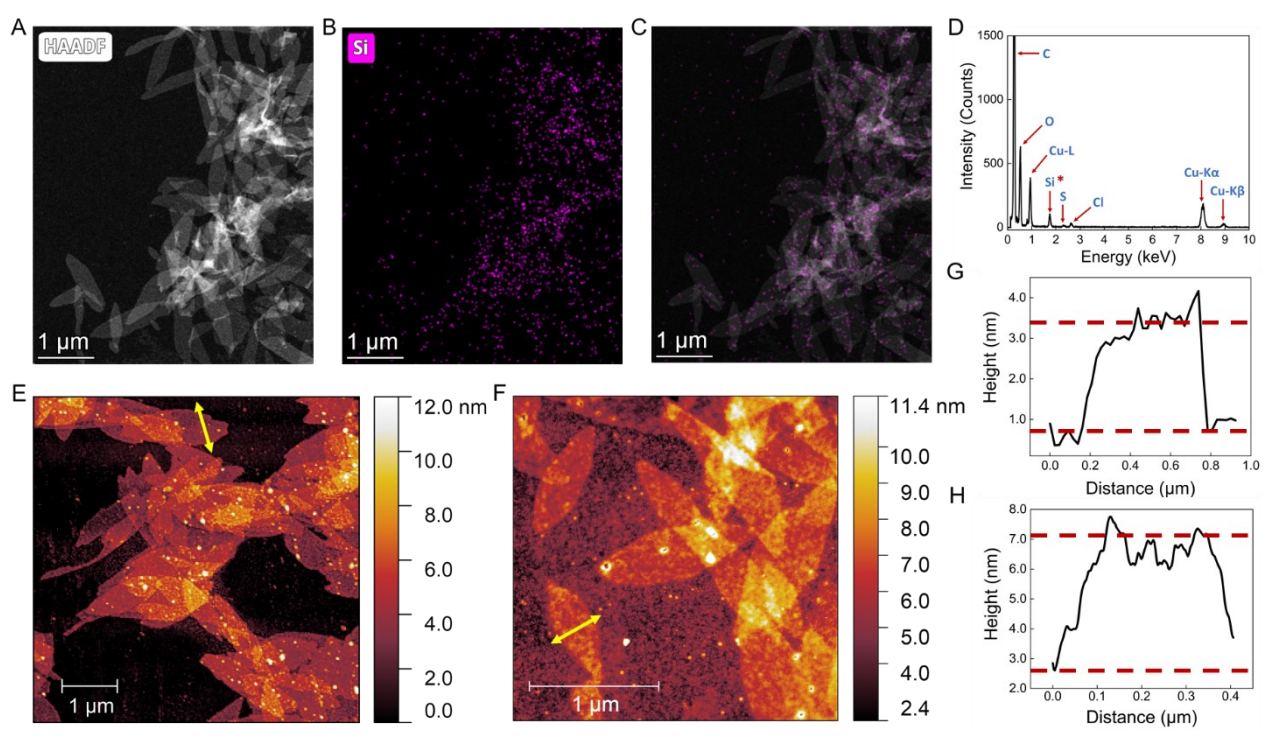


Figure 2. Surface analysis of silica-encapsulated TDBC J-aggregate sheets. (A) HAADF-STEM image of silica-encapsulated two-dimensional J-aggregate sheets. (B) EDX elemental map showing the silicon (Si) distribution within the field of view in (A). (C) overlap of (A) and (B) for better visual identification of homogeneous silica-encapsulation on the surface of J-aggregate sheets. Scale bar: 1 μm. (D) Integral EDX spectrum with the starred peak corresponding to silicon. J-aggregate solution was dried on 200-mesh copper grids covered with quantifoil holey carbon support films. Sharp peaks for C and Cu are expected. TDBC monomer contains S and Cl. In addition to these elemental peaks, silicon making an appearance indicates the presence of silicon in the sample. (E) and (F) AFM images of bare and silica-encapsulated TDBC J-aggregates, respectively. The height profiles along the yellow two headed arrows on (E) and (F) are shown, respectively in (G) and (H). The average thickness of a single J-aggregate sheet is approximately 2.7 nm while the formed silica coating on the surface adds an extra thickness of approximately 2 nm for the encapsulated J-aggregates.

Elemental mapping of silicon along with the overlap of HAADF-STEM images is consistent with homogeneous silica growth on the surfaces of TDBC J-aggregate sheets, as the denser distribution of silicon considerably overlaps with the J-aggregate region (Figs. 2B, 2C). The mechanical stability of the silica-encapsulated J-aggregates increased as shown in Fig. 2A; drying in air did not damage or disturb the sheet morphology. STEM-EDX analysis of silica-encapsulated TDBC J-aggregate sheets that were drop cast and dried on a hot plate confirmed homogeneous silica-encapsulation but had a distorted shape (refer to Fig. S3).

Atomic force microscopy (AFM) studies of bare and silica-encapsulated TDBC J-aggregate sheets and the resulting surface topography images are presented in Fig. 2E and 2F, respectively. Some sheets tend to stack, fold and overlap upon drying and adsorption onto the silica substrate, creating regions rich in J-aggregates. An analysis of the height profile of a bare J-aggregate sheet reveals an average thickness of ~2.7 nm (Fig. 2G), while that of a silica-encapsulated J-aggregate sheet is ~4.5 nm. Consequently, an additional thickness of ~2 nm silica is added to the sheet. The sheath thickness in silica-encapsulated TPPS J-aggregates has been reported to linearly vary in the range of 2 - 11 nm as the concentrations of silica precursors increase.³⁴

The excitonic coupling in J-aggregates is sensitive to the spatial arrangement of the chromophores. Strong excitonic coupling, due to significant overlap of molecular orbitals between adjacent chromophores, leads to a significant red shift in the absorption of J-aggregates. Long-range excitonic coupling, resulting from the alignment of transition dipoles of monomers over long distances, forms delocalized Frenkel excitons, leading to narrow linewidths and ultrafast excitonic transport. 44 The AFM height profile of the bare TDBC J-aggregate sheets aids in determining the molecular stacking geometry within the TDBC J-aggregate sheets. The three basic monomer arrangements in J-aggregates include staircase, ladder, and brickwork geometries. 40,45 The probable molecular geometry of the two-dimensional TDBC J-aggregate sheets is identified as the staircase arrangement, with molecular planes oriented normally to and along the long axis of the supramolecular lattice structure. When the monomers are stacked in the anti-parallel directions with a vertical molecular orientation, the efficient overlap of delocalized π -electron clouds is achieved through a slight lateral displacement of adjacent molecules, known as slippage (S).⁴⁵ This non-zero slippage generates a slip angle (α), $\alpha = atan(D/S)$, where D represents the distance between two adjacent monomer planes. According to the Avogadro Molecule Editor and Visualizer (Fig. S4), the height of a TDBC dye molecule is \sim 1.6 nm (Fig. 3A) while AFM reveals that the thickness of a bare J-aggregate sheet is ~2.7 nm (Fig. 3B and 3C). 40,46 Therefore, to agree with this height difference, the TDBC molecules must be in a vertical, anti-parallel, slightly staggered and non-linear arrangement, as shown in edge view (Fig. 3D). The long axes of the TDBC monomers are aligned parallel to each other and to the long axis of the J-aggregates, while the monomer planes are arranged perpendicular to the plane of the sheet (Fig. 3E). The bilaterally exposed polar sulfobutyl chains contribute to stabilizing the self-assembled structure in the aqueous medium while enabling silica-encapsulation from both the top and bottom sides of the sheets. A clearer representation of the monomer arrangement is given in Fig. S5. As sulfonate

groups extend from either side of the J-aggregate sheet, APTES is adsorbed on both sides, facilitating the formation of a silica sheath around the two-dimensional lattice and effectively protecting the J-aggregates from the external environment. The experimental data confirm the formation of an \sim 1 nm thick silica coating. The slip angle is measured by considering the acute angle at the vertices of TDBC sheets observed through AFM topography images. ^{45,47} The average slip angle is \sim 30 - 40° for bare TDBC J-aggregate sheets. Using Avogadro structural analysis, the slippage of adjacent monomers, (S), was measured to be \sim 1.2 nm (Fig. S4), resulting in an intermonomer spacing (D) of \sim 0.7 - 1.0 nm.

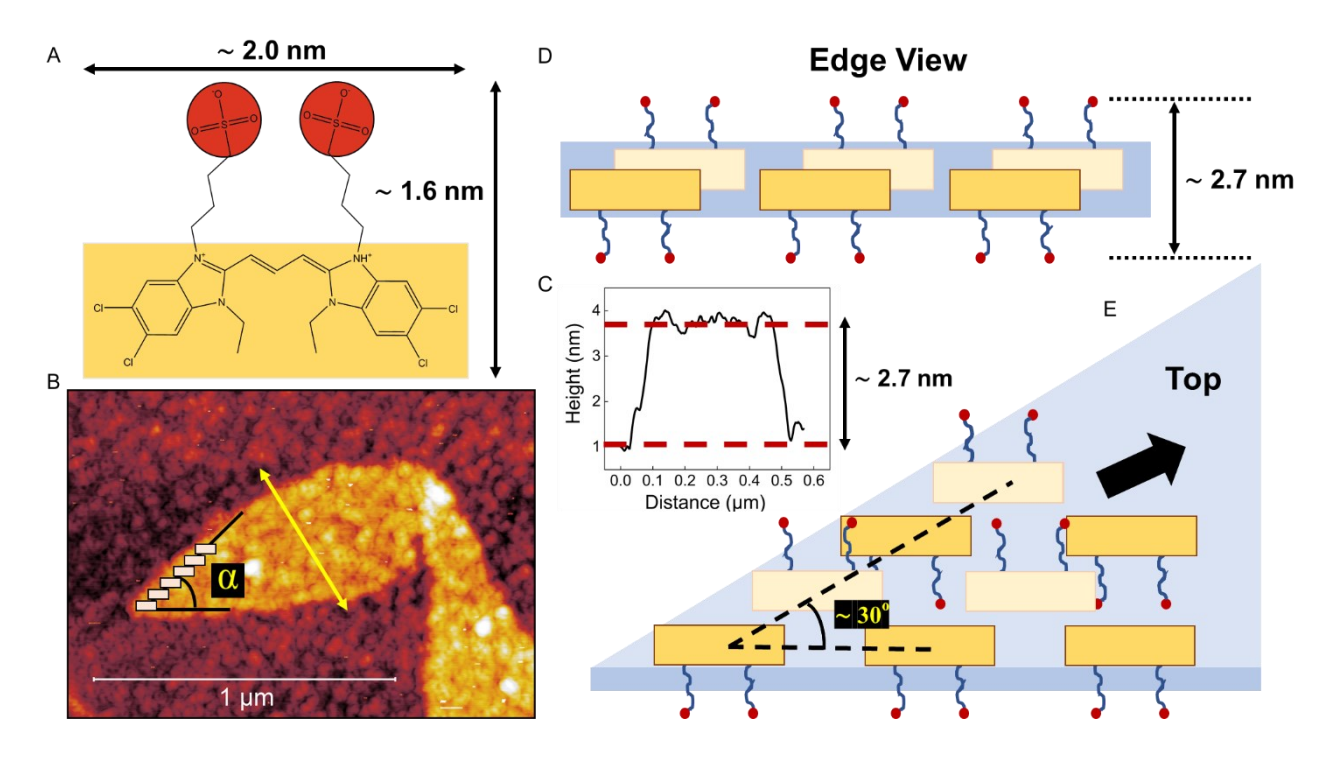


Figure 3. Structural model detailing the monomer arrangement within bare TDBC J-aggregate sheets. (A) Structure of TDBC monomer and its dimensions with mostly extended sulfobutyl groups obtained from the Avogadro molecule editor and visualizer. (B) AFM topography image of a bare J-aggregate sheet. Scale: 1 μ m. Schematic diagram illustrates the staircase arrangement of TDBC monomers and the slippage angle (α). (C) The height profile along the yellow two-headed arrow in (B). (D) Edge view of the structural model showcases vertical, anti-parallel, slightly staggered, and non-linear geometry of monomers, resulting in a \sim 2.7 nm thickness, consistent with the experimental AFM sheet thickness measurement. (E) Top view displays the monomer arrangement with the slip angle, caused by the lateral displacement of monomers. Black arrow indicates the direction of aggregate growth. Bilaterally exposed sulfobutyl groups allow silica-encapsulation from both the top and bottom surfaces of J-aggregate sheets.

Structural stability and optical enhancement through silica-encapsulation

The formation of a silica sheath, covering the entire J-aggregate, effectively shields it from external environmental stresses. This protective mechanism was experimentally verified through extensive dilution of stock solutions of bare (Fig. 4A) and silica-encapsulated (Fig. 4B) J-aggregates in ultrapure water. During the dilution process, ultrapure water was carefully added to the J-aggregate

stock solution, ensuring that the assembly of the already formed J-aggregates remained undisturbed. The J-aggregate/monomer ratio, obtained from the integrated absorption spectra (areas corresponding to 400 - 550 nm for the monomer and 551 - 650 nm for the J-aggregates), was plotted as a function of the dilution factor for both the bare and silica-encapsulated J-aggregates (Fig. 4C). Notably, a sharp decrease in the J-aggregate/monomer ratio for bare J-aggregates at a 25-fold dilution underscores the structural fragility of bare-J-aggregates. The mechanical stress induced by dilution prompts the ready disassembly of bare J-aggregates into their monomers, as indicated by the prominent absorption peak at 517 nm in Fig. 4A, corresponding to TDBC monomers. In contrast, silica-encapsulated J-aggregates exhibit increased robustness, retaining structural integrity without substantial disintegration even at a 125-fold dilution. This robustness resulting from silica-encapsulation ensures the structural stability of the TDBC J-aggregates under extensive dilution.

The photoluminescence QY of TDBC J-aggregates was measured using the reference method with a solution of rhodamine 6G in methanol (QY of 93%) as the standard.⁴⁸ The detailed QY calculation is given in Fig. S6. TDBC J-aggregates were formed from monomers that were purified prior to their self-assembly following a previously established method.²⁵ The QY enhancement was achieved by removing impurity sites that act as non-radiative recombination centers. Increasing the number of purification steps to three did not result in a substantial improvement in the QY of bare J-aggregates, moving from 82% to 88% (Fig. 4D).²⁵ The QY for silica-encapsulated TDBC J-aggregates from purified monomers was, in turn, 98% (Fig. 4E). As a control experiment, the same experiment was conducted for silica-encapsulated TDBC J-aggregates formed without any prior monomer purification. Surprisingly, the photoluminescence QY of bare J-aggregates from monomers as received without any prior purification was enhanced from 56% to 86% by encapsulation alone (Fig. 4F) showing that the silica-encapsulation process itself optically enhances TDBC J-aggregates without the essential need for monomer purification. Furthermore, silica-encapsulated TDBC J-aggregates maintain a stable QY over the course of 4-5 weeks when sealed and stored in the dark, wrapped with aluminum foil. By the end of the fifth week (day 35), silica-encapsulated TDBC J-aggregates record a 96% photoluminescence QY (Fig. S7). The photoluminescence QY of bare TDBC J-aggregates enhance over time due to self-annealing at room temperature but start photodegrading after 9 days of preparation.²⁵ Therefore, the silica layer adds extra photo stability to TDBC J-aggregates by acting as a protecting layer.

The enhancement in QY through silica-encapsulation can be explained by three factors. (I) APTES plays a dual role as a silica precursor and a primary amine, concentrating monomers before self-assembly and, as reported previously, enhances the QY by an order of magnitude. As illustrated in Fig. 1, our silica-encapsulation procedure, in contrast to previously reported methods, involves the formation of J-aggregates in the presence of APTES by first concentrating the monomers in the APTES phase. The non-aggregated monomeric form of TDBC is soluble in the amine phase, but due to its amphiphilic nature, J-aggregation occurs along the water-amine interface. Additionally, any monomers loosely bound to J-aggregates, potentially causing faulty stacking or

defects, are expected to dissolve in the amine phase, allowing pristing J-aggregate growth. (II) Silica precursors promote defect-free molecular packing in a similar way that previous works introduce small molecules and surfactants to promote defect-free close packing of monomers, which results in an increase of the QY. 49,50 In our method, as J-aggregates self-assemble, supramolecular lattice voids are filled by electrostatically adsorbing APTES, thus promoting dense molecular packing within the J-aggregates and strong coupling between chromophores. (III) Silica-encapsulation leads to the formation of smaller J-aggregate sheets. This reduction in physical size is attributed to the self-assembly of J-aggregates in the water-APTES bi-continuous phase, 49 the mechanical disturbance induced by silica mineralization, 34 and the controlled growth of J-aggregates in the presence of ammonium.⁴³ The controlled size of the J-aggregates limits the availability of non-radiative recombination sites, thereby enhancing radiative recombination and the photoluminescence OY. Collectively, these three factors explain the near-unity OYs observed in our silica-encapsulated J-aggregates. Furthermore, the high QY observed for silica-encapsulated J-aggregates from unpurified monomers may be attributed to in situ purification of monomers at the water-APTES bi-continuous interface during self-assembly. By reducing non-radiative decay channels and promoting efficient exciton transport and emission dynamics, silica-encapsulation significantly enhances the optical properties of TDBC J-aggregates.

The time-resolved fluorescence decay of bare J-aggregates from purified monomers follows a mono-exponential curve with a lifetime of 184 ps (Fig. 4G). This is slightly longer than the 174 ps emission lifetime earlier reported for J-aggregates formed from one-time purified monomers. Silica-encapsulated J-aggregates from both purified and unpurified monomers display emissive lifetimes of 234 ps and 226 ps, respectively. Using the QY and emissive lifetime data, we calculate the radiative and non-radiative rates for bare and silica-encapsulated J-aggregates, with and without prior monomer purification, as tabulated below (Table 1).

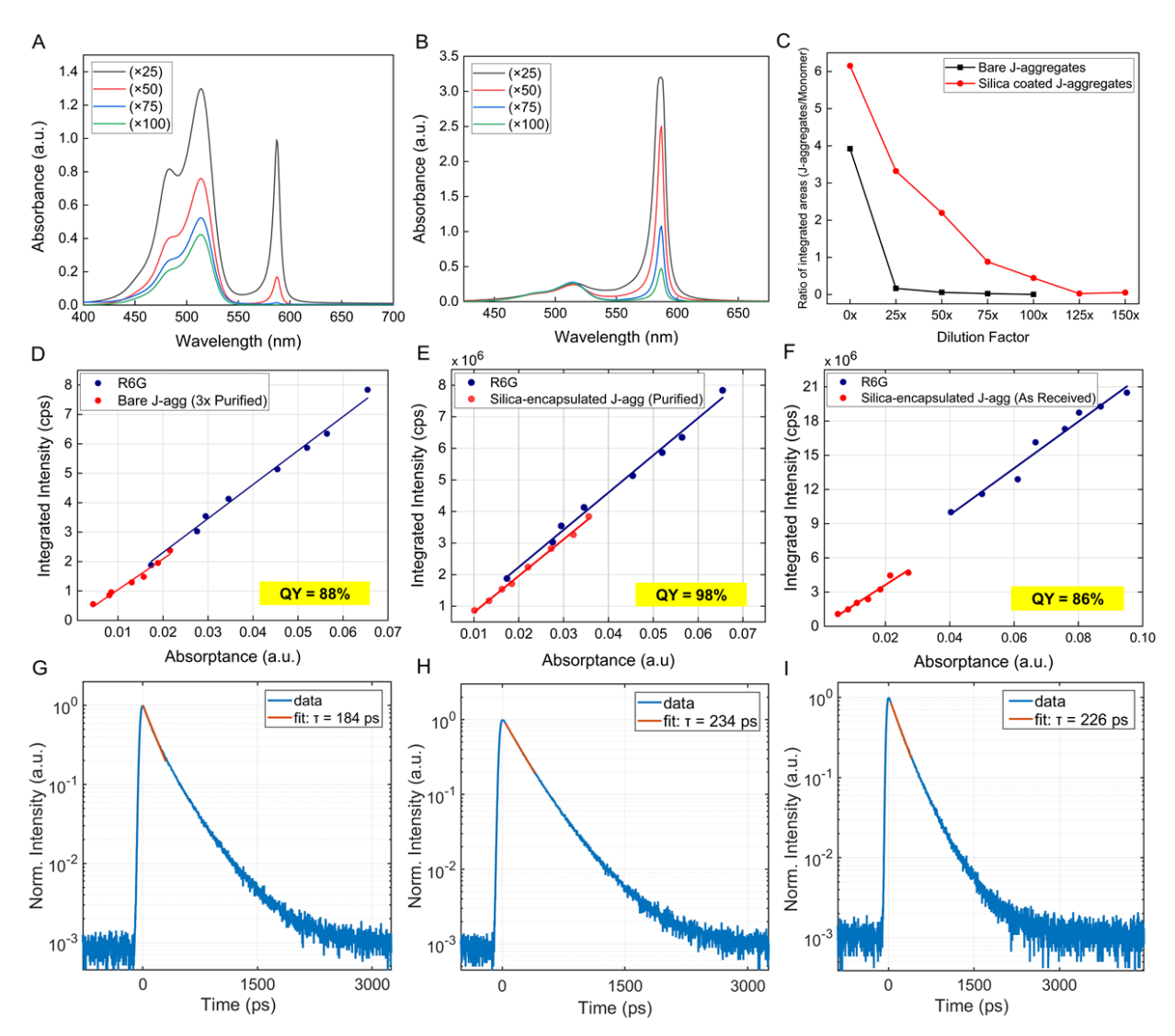


Figure 4. Structural stability and optical enhancement of TDBC J-aggregates through silicaencapsulation. Steady-state absorption for a dilution series of bare (A) and silica-encapsulated (B) TDBC J-aggregates. The dilution factors with respect to the initial TDBC dye concentration is mentioned in brackets. (C) J-aggregate/monomer ratio of integrated areas obtained from (A) and (B) as a function of dilution factor for bare (black) and silica-encapsulated (red) J-aggregates. The sharp fall in the Jaggregate/monomer ratio for bare J-aggregates upon 25 times dilution indicates the structural fragileness of bare-J-aggregates. Plot of integrated emission as a function of absorptance for rhodamine 6G (blue) and (D) bare J-aggregates from 3 times purified monomers using a previously established method²⁵, (E) silica-encapsulated J-aggregates from purified monomers, and (F) silica-encapsulated J-aggregates from monomers as received without any prior purification (red). Using the relative method⁴⁸ the OY is calculated to be 88% for J-aggregates from purified monomers, 98% for silica-encapsulated J-aggregates from purified monomers, and 86% for silica-encapsulated J-aggregates from monomers as received. Time-resolved fluorescence intensity of (G) bare J-aggregates from 3 times purified monomers ($\tau = 184$ ps), (H) silica-encapsulated J-aggregates from purified monomers ($\tau = 234$ ps), (I) silica-encapsulated Jaggregates from monomers as received without any prior purification ($\tau = 226$ ps) in blue with monoexponential fits in red. Excitation wavelength: 565 nm.

Table 1. QY, emissive lifetime, radiative and non-radiative rates for bare TDBC J-aggregates formed from monomers as received and purified and for silica-encapsulated TDBC J-aggregates formed from monomers as received and purified.

TDBC J-aggregate Type	Quantum Yield (φ)	Emissive Lifetime (τ)	Radiative Rate (<i>k_{rad}</i>)	Non-radiative Rate (k _{non-rad})
Bare J-aggregates without monomer purification	56%	167 ps	$3.4 \cdot 10^9 s^{-1}$	$2.6 \cdot 10^9 s^{-1}$
Bare J-aggregates with monomer purification	88 %	184 ps	$4.8 \cdot 10^9 s^{-1}$	$6.5 \cdot 10^8 s^{-1}$
Silica-encapsulated J- aggregates without monomer purification	86 %	226 ps	$3.8 \cdot 10^9 s^{-1}$	$6.2 \cdot 10^8 s^{-1}$
Silica-encapsulated J- aggregates with monomer purification	98 %	234 ps	$4.2 \cdot 10^9 s^{-1}$	$8.5 \cdot 10^7 s^{-1}$

We calculated the radiative rate of TDBC J-aggregates formed from repetitively purified monomers to be approximately 1.4 times faster than the radiative rate of J-aggregates formed from monomers as received without any prior purification. The rates shown in Table 1 emphasize that both monomer purification and silica-encapsulation enhance the radiative rate, with monomer purification contributing the most. This is consistent with the growth of more pristine and coherent J-aggregates. Bare and silica-encapsulated J-aggregates, both with monomer purification, display higher radiative rates, confirming our previous hypothesis that a significant portion of the non-radiative decay in J-aggregates is due to impurity quenchers. Therefore, we suggest a combined approach in which monomers are initially purified before encapsulation to produce bright and fast emitters with unity QYs. The highest non-radiative rate is recorded for bare J-aggregates formed from unpurified monomers. Through the individual processes of purification and silica-encapsulation, this non-radiative rate is reduced by a factor of 4. However, the combined process of monomer purification and silica-encapsulation reduces the non-radiative rate by a factor of approximately 31.

Temperature-dependent absorption and emission spectroscopy of silica-encapsulated TDBC J-aggregates

Kasha developed a model to explain the type of coupling in one-dimensional molecular aggregates based on spectral shifts compared to their monomers. The red or blue shift observed for molecular aggregates relative to their monomer peaks confirms negative or positive excitonic coupling in J- and H- type one-dimensional aggregates, respectively. However, Kasha's model cannot fully elucidate more complex excitonic behavior in two-dimensional aggregates, where the aggregate bright state could be lower in energy but still away from the band-edge, deviating from the J- aggregate nature, and referred to as I-aggregates. This behavior depends upon the relative slippage between neighboring monomers in the supramolecular assembly. ⁵¹

Temperature-dependent absorption and emission spectroscopy enables differentiation between Jand I- type coupling. 51,52 In this study, as we formed aggregates in the presence of the primary silica precursor, APTES, it was important to verify the coupling type of the resulting silicaencapsulated TDBC J-aggregates. Therefore, silica-encapsulated TDBC J-aggregates were further characterized by stabilizing them in a sugar matrix, facilitating temperature dependent measurements.^{53,54} This method involves diluting the silica-encapsulated J-aggregates in a concentrated sucrose-trehalose solution (1:1 w/w%) and drying overnight under vacuum. The sugar matrix forms an amorphous and glassy layer on top of the silica-encapsulated J-aggregates, acting as a cryoprotectant. This matrix effectively shields the silica-encapsulated J-aggregates from cryogenic damage, thereby enabling reliable cryogenic measurements. Further it reduces photobleaching and minimizes the re-absorption in J-aggregate thin films. The sugar matrix-fixed silica-encapsulated J-aggregates continued to fluoresce even after being exposed to air and natural daylight for several days. The unaffected absorption and emission spectral features of the sugar matrix-fixed silica-encapsulated J-aggregates confirmed that the water removal process does not affect the structure or morphology of the J-aggregates. This method has been successfully employed in studying the temperature-dependent absorption and emission spectra of TDBC and Cy3UB J-aggregates. 25,55 As the temperature decreases from 298 K to 79 K, both the absorbance and emission peaks exhibit a blue shift from 17,017 cm⁻¹ to 17,138 cm⁻¹ (from 587.7 nm to 583.5 nm) and 16,980 cm⁻¹ to 17,105 cm⁻¹ (from 589.0 nm to 584.6 nm), respectively (Figs. 5A and 5B). The blue shift in the absorption and emission spectra is clearly illustrated by plotting the peak absorption and emission against temperature in Fig. 5C. We observe an increase in the intensity of both the absorption and emission spectra upon cooling. The absorbance and emission line widths show narrowing upon cooling, from 233.9 cm⁻¹ to 193.7 cm⁻¹ (8.1 nm to 6.6 nm) and from 254.8 cm⁻¹ to 128.8 cm⁻¹ (8.8 nm to 4.4 nm), respectively (Figs. 5D and 5E). The absorption and emission peak positions and thermal broadening of silica-encapsulated TDBC J-aggregates red shift with increasing temperature. These observations are consistent with temperature-dependent spectroscopy of bare TDBC J-aggregates and consistent with J-type coupling between monomers.²⁵

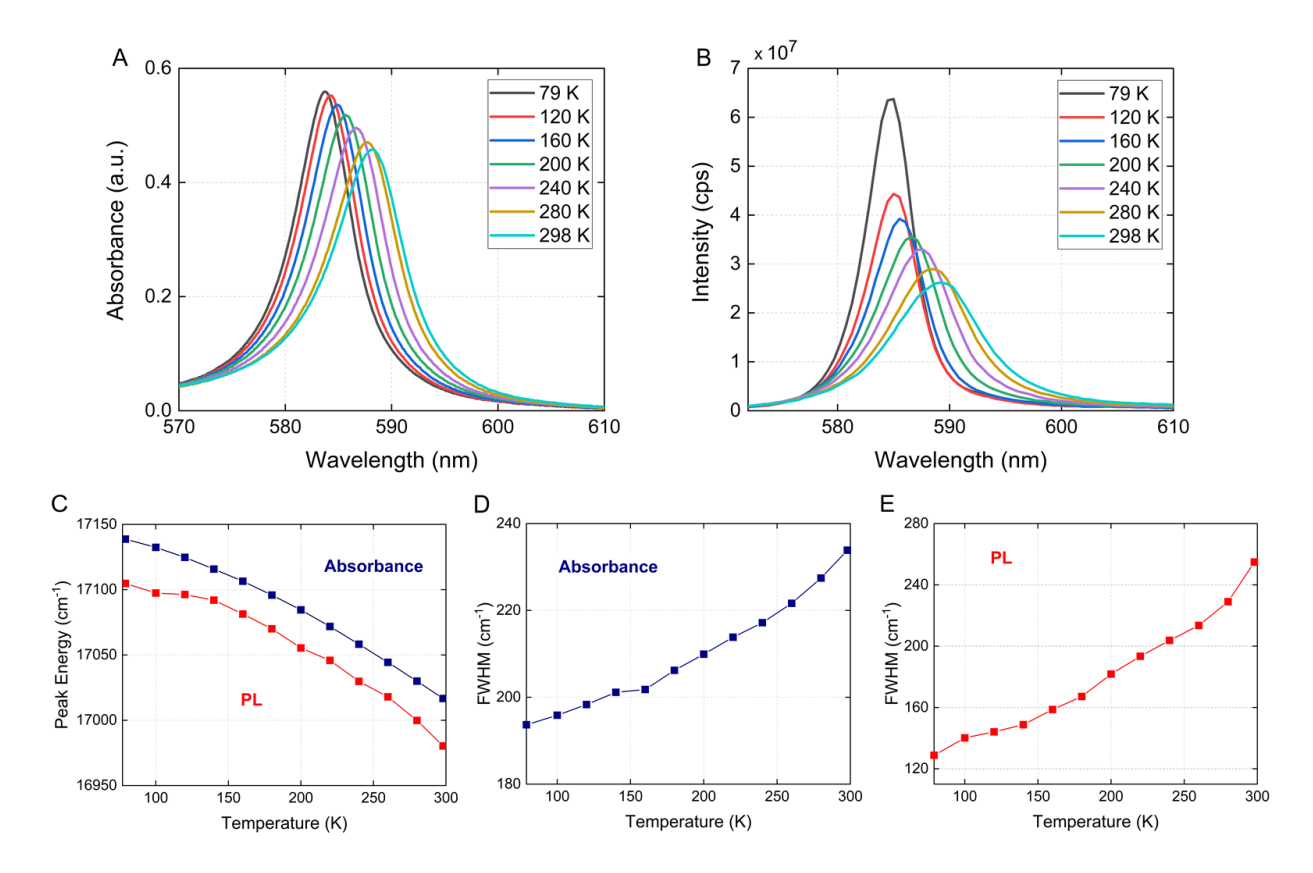


Figure 5. Temperature-dependent spectroscopy of silica-encapsulated TDBC J-aggregates in a dried sugar matrix. **(A)** Temperature-dependent absorption and emission spectra revealing a blue shift, narrowing, and intensification of J-aggregate absorption as the temperature decreases. **(B)** Temperature-dependent emission spectra revealing a blue shift, narrowing, and intensification of J-aggregate emission as the temperature decreases. Excitation wavelength: 532 nm. **(C)** Plot of peak absorption and emission energies as a function of temperature. **(D)** Plot of absorbance FWHM as a function of temperature. **(E)** Plot of fluorescence FWHM as a function of temperature.

CONCLUSION

In summary, we have substantially improved the structural stability and optical efficiency of two-dimensional sheet-like TDBC J-aggregates by encapsulating them in silica. The silica precursors APTES and TEOS together form an amorphous silica shell covering both the top and bottom of the J-aggregate sheets protecting them from external stresses. APTES plays a dual role by acting both as a silica precursor and a primary amine. The self-assembly of J-aggregates in the presence of APTES aids in molecular level *in situ* purification of monomers, and provides a monomer enriched phase enabling defect-free pristine J-aggregate formation. Aqueous ammonia catalyzes the hydrolysis of silica precursors and limits further J-aggregate growth, resulting in smaller lateral sizes for silica-encapsulated J-aggregates, as visualized by cryo-TEM and confirmed by DLS.

Additionally, silica-encapsulation provides a template for the assembly of TDBC monomers, encouraging further aggregation. We provide evidence for homogeneous silica coating on Jaggregate sheets through STEM-EDX elemental mapping. Furthermore, we discuss the probable staircase monomer architecture for TDBC J-aggregate sheets by incorporating both AFM experimental data and molecular dimensions. According to the AFM height profiles, the thickness of the TDBC bare J-aggregate sheet is approximately 2.7 nm, and we have successfully deposited a silica coating with an average thickness of 0.5 - 1 nm. By varying the silica-precursor concentration, the shell thickness can be controlled.

Silica-encapsulated J-aggregates survive up to 125-fold dilution in water, confirming the structural robustness of silica-encapsulation, which allows for future spectroscopic investigations of isolated Both purification and silica-encapsulation alone resulted in photoluminescence QYs. However, we report a near-unity photoluminescence QY of 98% with a 234 ps emissive lifetime for silica-encapsulated TDBC J-aggregates formed from purified monomers. The combination of monomer purification and encapsulation results in J-aggregates with the lowest non-radiative rate, $8.5 \cdot 10^7$ s⁻¹, which is 31 times lower than that of bare Jaggregates formed from unpurified monomers. Finally, we present temperature-dependent absorption and emission spectroscopy studies on silica-encapsulated TDBC J-aggregates to confirm the J-type coupling. Silica-encapsulation provides a platform for further surface functionalization of J-aggregates and integration with other optical materials. This approach provides a platform for fundamental studies of exciton delocalization, transport, and emission dynamics within a rigid matrix. Therefore, we conclude that silica-encapsulated TDBC Jaggregates are a building block fluorophore that is bright, fast, and robust. The findings from this study offer potential to advance the field and expand practical device applications of these intriguing superradiant supramolecular systems.

METHODS

Purification of TDBC monomers

Unless otherwise noted, all J-aggregate samples were prepared using purified TDBC monomers, following a slightly modified purification procedure provided by Ulugbek *et al.*²⁵ Initially, 150 mg of TDBC, as received from the vendor (FEW Chemicals, S0046), was dispersed in 25 mL methanol (>99.9%, VWR, EM-MX0488-1), and the resulting mixture was heated for 2 hours at 60 °C. Afterwards, the mixture was slowly cooled to room temperature overnight in the dark. The supernatant was carefully removed without disturbing the suspension, and the solid was dried at 70 °C, yielding 88 mg of the washed sample. This one-time washed sample was then dispersed again in 14 mL of methanol, and the purification step was repeated to yield 64.5 mg. During the third purification step, the solid from the second washing was dispersed in a 10 mL mixture of methanol and water (19:1, v/v), and the purification step was repeated. The dried, three-fold purified solid weighed 52 mg, resulting in a total yield of 35%.

Preparation of bare TDBC J-aggregates

A 6.5 mL mixture of methanol and water (12:1, v/v) was added to a vial containing 3.2 mg of purified TDBC solid. After being covered with aluminum foil, the vial was heated at 60 °C for 1 hr to prepare 0.65 mM monomer stock solution. For the J-aggregate stock solution, 550 μL of ultrapure water (Milli-Q, 18 MΩ·cm, Thermo Fisher Scientific) was added to 175 μL of the monomer stock solution in a cleaned vial. After gentle shaking and vortexing a few times a homogeneous pink-colored J-aggregate solution was obtained. J-aggregates from unpurified monomers were also prepared using the same procedure excluding the purification step. Unless otherwise specified, all the measurements were taken after equilibrating the solution overnight in the dark. To minimize J-aggregate exposure to light, the vials were wrapped in aluminum foil and stored in the dark.

Preparation of silica-encapsulated TDBC J-aggregates

Silica-encapsulated J-aggregates were prepared using modified literature methods. 33,35,56 The procedure was carried out inside a glove bag. APTES and TEOS were diluted in 1:49 v/v methanol solutions. In a cleaned vial, $10~\mu L$ of diluted APTES was added to $500~\mu L$ of ultrapure water and shaken well for several minutes to form an APTES-water solution blend. Subsequently, $175~\mu L$ of the TDBC monomer stock solution was added and vigorously shaken. Next, $10~\mu L$ of diluted TEOS and $10~\mu L$ of ultrapure water (to adjust the concentration) were added to the solution and mixed well. Afterwards, $20~\mu L$ of ammonium hydroxide was added, and the solution was mechanically shaken and vortexed at the maximum speed several times. The vial was then wrapped in aluminum foil, and the silica-encapsulated J-aggregate solution was kept in the dark overnight before any measurements were taken. Silica-encapsulated J-aggregates from unpurified monomers were prepared following the same procedure using the unpurified monomer stock.

Absorption and fluorescence spectroscopy

Absorption and emission spectra were recorded using a Cary 5000 Spectrometer (Agilent) and FluoroMax Fluorometer (Horiba Scientific), respectively. Spectra were collected by depositing an appropriate volume (50-60 μL , with excess wiped off after deposition) of bare and silicaencapsulated J-aggregate stock solutions in demountable quartz cuvettes with 0.1 mm path length (Starna). Dilution studies were conducted by carefully diluting both the bare and silicaencapsulated J-aggregate stock solutions in ultrapure water. During the preparation of the dilution series, ultrapure water was slowly added along the vial wall to meet the J-aggregate stock solution at the surface without encouraging the disassembly of already formed J-aggregates. Absorption and emission measurements were taken after allowing the diluted solutions to equilibrate for approximately 4 hours. Temperature-dependent absorption and emission spectroscopy was performed on silica-encapsulated TDBC J-aggregates fixed in a sugar matrix. The saturated sugar solution was prepared by adding 1.5 mL of ultrapure water to a 2 g solid mixture of sucrose (Sigma) and trehalose (Sigma) (1:1 w/w) and vigorously mixing by vortexing. A 100 μL aliquot of the silica-encapsulated TDBC J-aggregate stock solution was diluted by adding 100 μL of

ultrapure water. After allowing the J-aggregate sample to equilibrate for 1 h, 200 µL of the sugar solution was slowly added to the diluted J-aggregate solution and mixed well to obtain a homogeneous solution. After 1 h, 60 µL of sugar matrix-fixed silica-encapsulated J-aggregate solution was deposited onto a 0.1 mm demountable quartz cuvette and dried under 0.5 atm vacuum for two nights. Once completely dry, the cuvette was covered with the top lid and placed in a cold finger cryostat (Janis Research Co., ST-100). The cryostat was evacuated using a turbo pump (Agilent, Varian 9698222) until the pressure decreased to $\leq 1.0 \times 10^{-5}$ Torr. Initially, the sample was cooled under a constant flow of liquid nitrogen and the temperature was raised and controlled using a Lakeshore 330 Autotuning temperature controller. The sample was equilibrated for 5 minutes at each temperature, and absorbance measurements were taken with excitation and emission slit widths set to 1 nm resolution. The temperature-dependent fluorescence spectra were collected using a home-built PL spectrometer with a silicon camera. The sample was excited using a 532 nm continuous diode laser (Thorlabs, CPS532). Sample photoluminescence was focused through the entrance of a monochromator (Teledyne Princeton Instrument, SP-3750), set with a 100 μm slit width (corresponding to ~0.5 nm PL spectral resolution), before striking a diffraction grating with a groove density of 50 g/mm and a blaze of 600 nm. Sample emission was then imaged using a thermoelectrically cooled silicon camera (Teledyne, PIXIS-100). The fluorescence measurements were obtained with a 100 ms camera exposure time and 10 exposures averaged per frame.

Dynamic light scattering measurements

A volume of 75 μ L of ultrapure water was added to 225 μ L of J-aggregate stock solution, and allowed to equilibrate for approximately 3 hours prior to DLS measurements. Correlograms for both bare and silica-encapsulated J-aggregates were collected using a Zetasizer Nano ZS90 (Malvern Instruments, Model: ZEN3690). The intensity distributions as a function of size for the bare and silica-encapsulated TDBC J-aggregates are given in Fig. S2.

Cryo-TEM imaging

Instead of conventional TEM, cryo-TEM was employed to visualize bare and silica-encapsulated TDBC J-aggregates in their native environment. Copper grids covered with Quantifoil holey carbon support films (Q225CR-35, Quantifoil R 3.5/1, 200 mesh, Cu) were hydrophilized by glow discharge in an Emitech K100X Glow Discharger for one minute at 20 mA. A volume of 3 μL of TDBC J-aggregate solution was applied onto a grid and blotted using a Vitrobot Mark IV (Thermo Fisher Scientific) to remove the excess solution, applying a blot force of 4 for 6 seconds. The blotted specimen was then flash-frozen by rapidly plunging it into liquid ethane at approximately -175 0 C to vitrify the aqueous solution. Afterwards, under liquid nitrogen, the grids were transferred to the liquid nitrogen-cooled autoloader of Talos Arctica G2 Cryo-TEM (Thermo Fisher Scientific). To prevent J-aggregate degradation, imaging was performed under a minimal dose of the electron beam. The microscope was operated at an acceleration voltage of 200 kV with a 15 second exposure time, and the total exposure of the specimen was limited to 10.4 electrons/Å².

All images were collected at a magnification of 22,000X using a Falcon 3EC direct electron detector (Thermo Fisher Scientific) operated in linear mode. To generate sufficient contrast, images were collected in the -15 to -10 µm defocus range.

Quantum yield (QY)

The relative method was employed to calculate the QY of the TDBC J-aggregates. ^{48,57,58} A methanol solution of rhodamine 6G (Sigma, 252433-250MG), with a known QY of 93%, served as the standard. ⁵⁹ A series of solutions with different concentrations were prepared by diluting a rhodamine 6G stock solution with methanol. Similarly, another concentration series of J-aggregates was prepared by gently diluting the J-aggregate stock solution with water. The solutions were allowed to equilibrate for 3 hours before the measurements. The samples were deposited on 0.1 mm quartz cuvettes, and absorption and emission spectra were collected. For fluorescence emission spectra, rhodamine 6G and J-aggregates were excited at 500 nm and 565 nm, respectively. The integrated emission intensity was plotted against the absorptance for each series, and the slopes of the calibration plots were calculated. The QY was then calculated by incorporating the slopes from the calibration plots, refractive indices and powers at different excitation wavelengths. This procedure was repeated for both bare and silica-encapsulated J-aggregates, with and without prior monomer purification.

Emissive lifetime measurements

Emissive lifetimes were measured for bare, silica-encapsulated J-aggregates formed from monomers with or without prior purification. The J-aggregate stock solution was gently diluted 30 times with ultrapure water and allowed to equilibrate for 3 hours before the emissive lifetime measurement. To maintain low optical density and minimize reabsorption, samples were prepared using capillary action in rectangular miniature hollow glass tubes (5012 Rectangle VitroTubesTM) with a path length of 0.100 mm. Emission lifetime measurements were performed on a homebuilt microscope. The samples were excited with a wavelength-tunable ultrafast laser (Toptica Photonics FemtoFiber Pro) tuned to 565 nm with a repetition rate of 80 MHz and a power of 2 μW. The sample exposure during the measurements was kept brief to mitigate photobleaching. The laser was spectrally cleaned using Semrock VersaChrome edgepass filters and the light was focused on the sample using an achromatic doublet (80 mm focal length; Thorlabs AC254-080-A-ML) and collected with another 80 mm achromatic doublet. The excitation filter was a Semrock VersaChrome longpass filter. The light was then sent to a single-photon avalanche photodiode (Micro Photon Devices), and timing was performed with a PicoQuant Hydraharp 400 module. Steady-state spectra were collected on a Princeton Instruments Acton SP2500 and focused onto a Princeton Instruments ProEM CCD array. Lifetime traces were obtained by integrating the emission across the wavelength range of 570-600 nm over a minute. All the data were analyzed with custom software written in Matlab.

STEM-EDX measurements

High-angle annular dark-field scanning transmission electron microscopy (HAADF-STEM) images and energy-dispersive X-ray spectroscopy (EDX) of silica-encapsulated J-aggregate sheets

were collected using a Thermo Fisher Scientific Themis Z G3 STEM operating at an acceleration

voltage of 200 kV, with a convergence angle of 19 mrad and 100 pA beam current. TEM grids

with a Formvar film coated with a heavier layer of carbon (Carbon Type-B, 01813-F) on a copper

300-mesh support were used. Samples were prepared by drop casting 20 µL of the silica-

encapsulated J-aggregate solution onto TEM grids without any additional dilution and were left to

dry at room temperature for a couple of hours before imaging.

AFM measurements

Atomic force microscopy (AFM) was carried out using a Cypher VRS1250 microscope operating

in tapping mode in air with a fast-scanning, high-frequency silicon probe from Asylum Research Oxford Instruments (FS1500AUD, 1500 kHz, 6 Nm⁻¹). The AFM images were processed, and the

height profiles were analyzed using Gwyddion software. Substrates for AFM were prepared by

spin-coating J-aggregate samples onto hydrophilized silica substrates at 1200 rpm for 2 minutes.

The spin-coating procedure was repeated, and 5 µL of J-aggregate stock solution was added at a time until a sufficient amount of sample was deposited on the substrate. The silica shell thickness

was determined by subtracting the average height of a bare-J-aggregate sheet from the height of a

silica-encapsulated sheet and dividing by two.

ASSOCIATED CONTENT

Supporting Information Available:

Normalized absorption and emission spectra of bare and silica-encapsulated TDBC J-aggregates, dynamic light scattering distribution of bare and silica-encapsulated J-aggregates, surface analysis

of silica-encapsulated TDBC J-aggregate sheets, molecular dimensions and monomer arrangement

of TDBC, quantum yield calculation of TDBC J-aggregates.

AUTHOR INFORMATION

Corresponding Author

*E-mail: mgb@mit.edu. Phone: 617-497-0458

20

ORCID

Dimuthu H. Thanippuli Arachchi: 0000-0003-4750-3951

Ulugbek Barotov: 0000-0002-8931-9127

Collin F. Perkinson: 0000-0002-5676-1998

Tara Šverko: 0000-0002-2046-9151

Alexander E. K. Kaplan: 0000-0003-2994-6134

Moungi G. Bawendi: 0000-0003-2220-4365

Notes: The authors declare no competing financial interest.

AUTHOR CONTRIBUTIONS

D. H. T. A. conceived the idea, developed the project, formulated the silica-encapsulation procedure, prepared the J-aggregate samples, performed optical and structural measurements and analyzed the data. U. B. helped in organizing the research idea, structuring the project and developing the J-aggregate sample preparation and measuring techniques. C. F. P. provided assistance in setting up the instrumentation and collecting the temperature dependent absorption and emission spectroscopy data. T. S. and A. E. K. K. developed the instrumentation for J-aggregate lifetime analysis, assisted lifetime measurements and analysis. D. H. T. A. wrote the manuscript and all of the authors provided insightful feedback and comments. M. G. B. directed and supervised the project.

ACKNOWLEDGMENTS

D. H. T. A. and U.B. acknowledge support from the National Science Foundation (award No. CHE-2108357). C. F. P., T. S. and A. E. K. K. acknowledge support from the US Department of Energy, Office of Basic Energy Sciences, Division of Materials Sciences and Engineering (award No. DE-SC0021650). T.S. also acknowledges support from a Graduate Fellowship from the Natural Sciences and Engineering Research Council of Canada (NSERC). We thank Christopher Borsa, Sarah Sterling, Rami Dana, Aubrey Penn, and the MIT.nano facility for providing assistance with cryo-TEM, AFM, STEM-EDX imaging and characterization.

REFERENCES

- (1) Würthner, F.; Kaiser, T. E.; Saha-Möller, C. R. J-Aggregates: From Serendipitous Discovery to Supramolecular Engineering of Functional Dye Materials. *Angewandte Chemie International Edition* **2011**, *50*, 3376–3410.
- (2) Shindy, H. A. Fundamentals in the Chemistry of Cyanine Dyes: A Review. *Dyes and Pigments* **2017**, *145*, 505–513.
- (3) Kirstein, S.; Daehne, S. J-Aggregates of Amphiphilic Cyanine Dyes: Self-Organization of Artificial Light Harvesting Complexes. *International Journal of Photoenergy* **2006**.
- (4) Augulis, R.; Pugžlys, A.; Van Loosdrecht, P. H. M. Exciton Dynamics in Molecular Aggregates. *Physica status solidi C* **2006**, *3*, 3400–3403.
- (5) Egorov, V. V. Theory of the J-Band: From the Frenkel Exciton to Charge Transfer. *Physics procedia* **2009**, *2*, 223–326.
- (6) Jelley, E. E. Spectral Absorption and Fluorescence of Dyes in the Molecular State. *Nature* **1936**, *138*, 1009-1010.
- (7) Scheibe, G. Über Die Veränderlichkeit Der Absorptionsspektren in Lösungen Und Die Nebenvalenzen Als Ihre Ursache. *Angewandte Chemie* **1937**, *50*, 212–219.
- (8) Sorokin, A. V.; Ropakova, I. Y.; Grynyov, R. S.; Vilkisky, M. M.; Liakh, V. M.; Borovoy, I. A.; Yefimova, S. L.; Malyukin, Y. V. Strong Difference between Optical Properties and Morphologies for J-Aggregates of Similar Cyanine Dyes. *Dyes and Pigments* 2018, 152, 49–53.
- (9) Kim, T.; Ham, S.; Lee, S. H.; Hong, Y.; Kim, D. Enhancement of Exciton Transport in Porphyrin Aggregate Nanostructures by Controlling the Hierarchical Self-Assembly. *Nanoscale* **2018**, *10*, 16438–16446.
- (10) Eisele, D. M.; Knoester, J.; Kirstein, S.; Rabe, J. P.; Vanden Bout, D. A. Uniform Exciton Fluorescence from Individual Molecular Nanotubes Immobilized on Solid Substrates. *Nat. nanotechnol* **2009**, *4*, 658–663.
- (11) Rhodes, S.; Liang, W.; Wang, X.; Reddy, N. R.; Fang, J. Transition from H-Aggregate Nanotubes to J-Aggregate Nanoribbons. *The Journal of Physical Chemistry C* **2020**, *124*, 11722–11729.
- (12) Spano, F. C.; Mukamel, S. Superradiance in Molecular Aggregates. *J Chem Phys* **1989**, *91*, 683–700.
- (13) Kasha, M. Energy Transfer Mechanisms and the Molecular Exciton Model for Molecular Aggregates. *Radiation research* **1963**, *20*, 55-70.
- (14) Han, J.; Zhang, H.; Abramavicius, D. Exchange Narrowing and Exciton Delocalization in Disordered J Aggregates: Simulated Peak Shapes in the Two Dimensional Spectra. *The Journal of Chemical Physics* **2013**, *139*.
- (15) Brixner, T.; Hildner, R.; Köhler, J.; Lambert, C.; Würthner, F. Exciton Transport in Molecular Aggregates From Natural Antennas to Synthetic Chromophore Systems. *Advanced Energy Materials* **2017**, *7*, 1700236.

- (16) Valleau, S.; Saikin, S. K.; Yung, M. H.; Guzik, A. A. Exciton Transport in Thin-Film Cyanine Dye J-Aggregates. *Journal of Chemical Physics* **2012**, *137*.
- (17) Zhao, Y.; Wang, V.; Javey, A. Molecular Materials with Short Radiative Lifetime for High-Speed Light-Emitting Devices. *Matter.* **2020**, *3*, 1832–1844.
- (18) Kemnitz, K.; Yoshihara, K.; Tani, T. Short and Excitation-Independent Fluorescence Lifetimes of J-Aggregates Adsorbed on AgBr and SiO2 sub 2. *Journal of Physical Chemistry* **1990**, *94*.
- (19) Eisele, D. M.; Cone, C. W.; Bloemsma, E. A.; Vlaming, S. M.; Van Der Kwaak, C. G. F.; Silbey, R. J.; Bawendi, M. G.; Knoester, J.; Rabe, J. P.; Vanden Bout, D. A. Utilizing Redox-Chemistry to Elucidate the Nature of Exciton Transitions in Supramolecular Dye Nanotubes. *Nat Chem* **2012**, *4*, 655–662.
- (20) Slavnova, T. D.; Görner, H.; Chibisov, A. K. Cyanine-Based J-Aggregates as a Chirality-Sensing Supramolecular System. *Journal of Physical Chemistry B* **2011**, *115*, 3379–3384.
- (21) Liang, W.; He, S.; Fang, J. Self-Assembly of J-Aggregate Nanotubes and Their Applications for Sensing Dopamine. *Langmuir* **2014**, *30*, 805–811.
- (22) Xu, S.; Liu, H. W.; Huan, S. Y.; Yuan, L.; Zhang, X. B. Recent Progress in Utilizing Near-Infrared J-Aggregates for Imaging and Cancer Therapy. *Materials Chemistry Frontiers* **2021**, *5*, 1076–1089.
- (23) Bricks, J. L.; Slominskii, Y. L.; Panas, I. D.; Demchenko, A. P. Fluorescent J-Aggregates of Cyanine Dyes: Basic Research and Applications Review. *Methods and Applications in Fluorescence* **2017**, *6*, 012001
- (24) Peyronel, T.; Quirk, K. J.; Wang, S. C.; Tiecke, T. G. Luminescent Detector for Free-Space Optical Communication. *Optica* **2016**, *3*, 787-792.
- (25) Barotov, U.; Thanippuli Arachchi, D. H.; Klein, M. D.; Zhang, J.; Šverko, T.; Bawendi, M. G. Near-Unity Superradiant Emission from Delocalized Frenkel Excitons in a Two-Dimensional Supramolecular Assembly. *Adv Opt Mater* **2023**, 11
- (26) Thilagam, A. Quantum information processing attributes of J-aggregates. In *J-Aggregates: Volume 2*. 2012; pp 273-308.
- (27) Sorokin, A. V.; Pereverzev, N. V.; Grankina, I. I.; Yefimova, S. L.; Malyukin, Y. V. Evidence of Exciton Self-Trapping in Pseudoisocyanine J-Aggregates Formed in Layered Polymer Films. *Journal of Physical Chemistry C* **2015**, *119*, 27865–27873.
- (28) Malyukin, Y. V.; Sorokin, A. V.; Semynozhenko, V. P. Features of Exciton Dynamics in Molecular Nanoclusters (J-Aggregates): Exciton self-trapping. *Low Temp. Phys.* **2016**, *42*, 429–440.
- (29) Meng, C.; Yang, D.; Wu, Y.; Zhang, X.; Zeng, H.; Li, X. Synthesis of Single CsPbBr3@SiO2 Core-Shell Particles: Via Surface Activation. *J. Mater. Chem. C* **2020**, 8, 17403–17409.
- (30) El-Nahhal, I. M.; Salem, J. K.; Kuhn, S.; Hammad, T.; Hempelmann, R.; Al Bhaisi, S. Synthesis and Characterization of Silica Coated and Functionalized Silica Coated Zinc Oxide Nanomaterials. *Powder Technology* **2016**, *287*, 439–446.

- (31) Park, J. C.; Gilbert, D. A.; Liu, K.; Louie, A. Y. Microwave Enhanced Silica Encapsulation of Magnetic Nanoparticles. *J. Mater. Chem.* **2012**, *22*, 8449–8454.
- (32) Ng, K.; Webster, M.; Carbery, W. P.; Visaveliya, N.; Gaikwad, P.; Jang, S. J.; Kretzschmar, I.; Eisele, D. M. Frenkel Excitons in Heat-Stressed Supramolecular Nanocomposites Enabled by Tunable Cage-like Scaffolding. *Nat Chem* **2020**, *12*, 1157–1164.
- (33) Qiao, Y.; Polzer, F.; Kirmse, H.; Kirstein, S.; Rabe, J. P. Nanohybrids from Nanotubular J-Aggregates and Transparent Silica Nanoshells. *Chemical Communications* **2015**, *51*, 11980–11982.
- (34) Gurunatha, K. L.; Dujardin, E. Tuning the Optical Coupling between Molecular Dyes and Metal Nanoparticles by the Templated Silica Mineralization of J-Aggregates. *J. Phys. Chem. C* **2013**, *117*, 3489–3496.
- (35) Herman, K., Kirmse, H., Eljarrat, A., Koch, C. T., Kirstein, S., & Rabe, J. P. Individual Tubular J-aggregates Stabilized and Stiffened by Silica Encapsulation. *Colloid and Polymer Science* **2020**, *298*, 937-950.
- (36) Moll, J.; Daehne, S.; Durrant, J. R.; Wiersma, D. A. Optical Dynamics of Excitons in J Aggregates of a Carbocyanine Dye. *J. Chem. Phys.* **1995**, *102*, 6362–6370.
- (37) Moll, J.; Daehne, S.; Durrant, J R; Wiersma, D. A. Exciton Dynamics in the J-Aggregates of a Carbocyanine Dye. *Journal of Fluorescence* **1994**, *4*, 57-59.
- (38) Hada, H., Hanawa, R., Haraguchi, A., & Yonezawa, Y. Preparation of the J-aggregate of Cyanine Dyes by Means of the Langmuir-Blodgett Technique. *J. Phys. Chem.* **1985**, *89*, 560-562.
- (39) Bailey, A. D.; Deshmukh, A. P.; Bradbury, N. C.; Pengshung, M.; Atallah, T. L.; Williams, J. A.; Barotov, U.; Neuhauser, D.; Sletten, E. M.; Caram, J. R.; Bailey, M. A.; Deshmukh, A.; Williams, J.; Bradbury, N.; Sletten, E.; Caram, J.; Atallah, T. Exploring the Design of Superradiant J-Aggregates from Amphiphilic Monomer Units. *Nanoscale* **2023**, *15*, 3841-3849.
- (40) Prokhorov, V. V.; Petrova, M. G.; Kovaleva, N. N.; Demikhov, E. I. Atomic Force and Scanning Near-Field Optical Microscopy Study of Carbocyanine Dye J-Aggregates. *Curr Nanosci* **2014**, *10*, 700–704.
- (41) Al-Khatib, O.; Böttcher, C.; Von Berlepsch, H.; Herman, K.; Schön, S.; Rabe, J. P.; Kirstein, S. Adsorption of Polyelectrolytes onto the Oppositely Charged Surface of Tubular J-Aggregates of a Cyanine Dye. *Colloid and Polymer Science* **2019**, *297*, 729-739.
- (42) Stöber, W., Fink, A., & Bohn, E. Controlled Growth of Monodisperse Silica Spheres in the Micron Size Range. *Journal of colloid and interface science* **1968**, 26, 62-69.
- (43) Koti, A. S. R.; Taneja, J.; Periasamy, N. Control of Coherence Length and Aggregate Size in the J-Aggregate of Porphyrin. *Chem Phys Lett* **2003**, *375*, 171–176.
- (44) Deshmukh, A. P.; Zheng, W.; Chuang, C.; Bailey, A. D.; Williams, J. A.; Sletten, E. M.; Egelman, E. H.; Caram, J. R. Near-Atomic-Resolution Structure of J-Aggregated Helical Light-Harvesting Nanotubes. *Nat. Chem.* **2024**, *16*, 800-808.

- (45) Prokhorov, V. V.; Pozin, S. I.; Lypenko, D. A.; Perelygina, O. M.; Mal'tsev, E. I.; Vannikov, A. V. Molecular Arrangements in Two-Dimensional J-Aggregate Monolayers of Cyanine Dyes. *Macroheterocycles* **2012**, *5*, 371–376.
- (46) Prokhorov, V. V.; Perelygina, O. M.; Pozin, S. I.; Mal'Tsev, E. I.; Vannikov, A. V. Polymorphism of Two-Dimensional Cyanine Dye J-Aggregates and Its Genesis: Fluorescence Microscopy and Atomic Force Microscopy Study. *J. Phys. Chem. B* 2015, 119, 15046–15053.
- (47) Prokhorov, V. V.; Perelygina, O. M.; Pozin, S. I.; Mal'Tsev, E. I.; Vannikov, A. V.; Tsivadze, A. Y. Tubular Structure of J-Aggregates of Cyanine Dye. *Doklady Chemistry* **2015**, *460*, 1–4.
- (48) Würth, C.; Grabolle, M.; Pauli, J.; Spieles, M.; Resch-Genger, U. Comparison of methods and achievable uncertainties for the relative and absolute measurement of photoluminescence quantum yields. *Anal. Chem.* **2011**, *83*, 3431-3439.
- (49) Anantharaman, S. B.; Kohlbrecher, J.; Rainò, G.; Yakunin, S.; Stöferle, T.; Patel, J.; Kovalenko, M.; Mahrt, R. F.; Nüesch, F. A.; Heier, J. Enhanced Room-Temperature Photoluminescence Quantum Yield in Morphology Controlled J-Aggregates. *Advanced Science* **2021**, *8*, 1903080.
- (50) Grankina, I. I.; Borovoy, I. A.; Petrushenko, S. I.; Hrankina, S. S.; Semynozhenko, V. P.; Yefimova, S. L.; Sorokin, A. V. Fluorescent Properties of Amphi-PIC J-Aggregates in the Complexes with Bovine Serum Albumin. *J. Mol. Liq.* **2022**, *368*, 120755.
- (51) Chuang, C.; Bennett, D. I. G.; Caram, J. R.; Aspuru-Guzik, A.; Bawendi, M. G.; Cao, J. Generalized Kasha's Model: T-Dependent Spectroscopy Reveals Short-Range Structures of 2D Excitonic Systems. *Chem* **2019**, *5*, 3135–3150.
- (52) Deshmukh, A. P.; Geue, N.; Bradbury, N. C.; Atallah, T. L.; Chuang, C.; Pengshung, M.; Cao, J.; Sletten, E. M.; Neuhauser, D.; Caram, J. R. Bridging the Gap between H- and J-Aggregates: Classification and Supramolecular Tunability for Excitonic Band Structures in Two-Dimensional Molecular Aggregates. *Chemical Physics Reviews* **2022**, *3*.
- (53) Doria, S.; Sinclair, T. S.; Klein, N. D.; Bennett, D. I. G.; Chuang, C.; Freyria, F. S.; Steiner, C. P.; Foggi, P.; Nelson, K. A.; Cao, J.; Aspuru-Guzik, A.; Lloyd, S.; Caram, J. R.; Bawendi, M. G. Photochemical Control of Exciton Superradiance in Light-Harvesting Nanotubes. ACS Nano 2018, 12, 4556–4564.
- (54) Caram, J. R.; Doria, S.; Eisele, D. M.; Freyria, F. S.; Sinclair, T. S.; Rebentrost, P.; Lloyd, S.; Bawendi, M. G. Room-Temperature Micron-Scale Exciton Migration in a Stabilized Emissive Molecular Aggregate. *Nano Lett* **2016**, *16*, 6808–6815.
- (55) Barotov, U.; Klein, M. D.; Wang, L.; Bawendi, M. G. Designing Highly Luminescent Molecular Aggregates via Bottom-Up Nanoscale Engineering. *J. Phys. Chem. C* **2021**, *126*, 754–763.
- (56) Klein, M. D.; Shulenberger, K. E.; Barotov, U.; Šverko, T.; Bawendi, M. G. Supramolecular Lattice Deformation and Exciton Trapping in Nanotubular J-Aggregates. *J. Phys. Chem. C* **2022**, *126*, 4095–4105.

- (57) Fennel, F.; Gershberg, J.; Stolte, M.; Würthner, F. Fluorescence Quantum Yields of Dye Aggregates: A Showcase Example Based on Self-Assembled Perylene Bisimide Dimers. *Physical Chemistry Chemical Physics* **2018**, *20*, 7612–7620.
- (58) Hu, J.; Zhang, C. Y. Simple and Accurate Quantification of Quantum Yield at the Single-Molecule/Particle Level. *Anal Chem* **2013**, *85*, 2000–2004.
- (59) Magde, D.; Wong, R.; Seybold, P. G. Fluorescence Quantum Yields and Their Relation to Lifetimes of Rhodamine 6G and Fluorescein in Nine Solvents: Improved Absolute Standards for Quantum Yields. *Photochem Photobiol* **2007**, *75*, 327–334.